Copper Electrodeposition Kinetics Measured by Alternating Current Voltammetry and the Role of Ferrous Species

Mary-Elizabeth Wagner,[a] Rodrigo Valenzuela,[b] Tomás Vargas,[b,c] Melanie Colet-Lagrille,[b,c] and Antoine Allanore[a,*,z]

[a]*Department of Materials Science and Engineering, Massachusetts Institute of Technology, Cambridge, Massachusetts 02139-4307, USA*
[b]*Laboratorio de Electroquímica, Departamento de Ingeniería Química y Biotecnología, Universidad de Chile, Santiago, Región Metropolitana, Chile*
[c]*Advanced Mining Technology Center (AMTC), Universidad de Chile, Santiago, Región Metropolitana, Chile*

Impurities and additives play a key role in copper electrodeposition, in particular in upstream processes such as electrowinning or electrorefining. One common impurity is iron, mostly present as iron species Fe(II) in highly concentrated sulfuric acid solutions and in a cathodic environment. Herein, the kinetics of copper electrodeposition from such solutions have been investigated using a copper rotating disk electrode and alternating current voltammetry (ACV). For a concentration of proton of 1.84 M and a concentration of Fe(II) ions of 0.054 M, the deposition kinetics are slow enough to separately observe the two electron transfer steps involved in copper reduction: an observation unique to ACV. The results suggest that Fe(II) ions affect the electrodeposition kinetic by slowing down reaction kinetics, in particular slowing the second electron transfer reaction.
 [DOI: 10.1149/2.0121602jes] All rights reserved.

Manuscript submitted July 8, 2015; revised manuscript received October 19, 2015. Published November 5, 2015.

Advancing the understanding of copper electrodeposition kinetics in a concentrated sulfuric acid electrolyte is beneficial at multiple stages of copper life cycle. At the extraction and purification stage, copper electrowinning and anode electrorefining are essential steps. In both cases, the metal deposited on the cathode needs to be periodically recovered, requiring the deposit to remain structurally stable throughout the duration of metal growth. In downstream copper applications, such as electronics manufacture, the presence of voids or the lack of sufficient nuclei coalescence in electrodeposits can ultimately compromise the integrity of products, e.g. computer chips. This last issue has recently been driving research to improve deposit quality,[1–3] but less work has been published on the challenges faced in upstream copper production.

Various factors influencing copper electrodeposition have been reported in conditions simulating the low pH, high copper concentration electrolytes common in industrial conditions.[4–6] In upstream steps such as electrowinning or electrorefining, solution additives play an important, though only marginally understood, role in the final deposit quality. Additives encompass both inevitable impurities inherited from the raw minerals and carried along with copper during the smelting process,[7] as well as impurities purposely added to improve the deposit properties.[8] The outcome on deposit quality varies widely,[6–10] with additives exhibiting either a positive or negative effect on copper growth. Of particular interest in this work, Fe(II) ions have been reported to have a positive effect,[3,6] possibly due to slowing down the reduction kinetics of copper.[9] Because upstream copper production involves deposition on copper cathodes, the present study is limited to copper deposition on a copper substrate. Thus, our study is not one of copper nucleation during electrodeposition, but rather speaks about electrodeposition kinetics during growth.

Electrodeposition is a complex process drawing on multi-physics, and the reduction process for the deposition of copper written as:

$$Cu^{2+} + 2e^- \rightarrow Cu \qquad [1]$$

actually involves many interrelated phenomena, such as mass transport, charge transfer, adatom diffusion, incorporation into growth sites, and crystallization, each governed by their own rates. The situation is further complicated for copper electrodeposition in concentrated electrolyte, where a four-step mechanism, commonly referred to as an (C)ECE reaction, is cited:[11]

$$Chemical\ reaction\ (C) \quad Cu^{2+}(H_2O)_6 \overset{-xH_2O}{\Longleftrightarrow} Cu^{2+}(H_2O)_{6-x} \qquad [2]$$

$$Electron\ transfer\ (E) \quad Cu^{2+}(H_2O)_{6-x} \overset{e^-}{\Leftrightarrow} Cu^{+}(H_2O)_{6-x} \qquad [3]$$

$$Chemical\ reaction\ (C) \quad Cu^{+}(H_2O)_{6-x} \begin{cases} \overset{-yH_2O}{\Longleftrightarrow} Cu^{+}(H_2O)_{6-x-y} \\ \overset{-zH_2O,H^+}{\Longleftrightarrow} Cu^{+}(H_2O)_{5-x-z}\,OH^- \end{cases} \qquad [4]$$

$$Electron\ transfer\ (E) \quad \left.\begin{matrix} Cu^{+}(H_2O)_{6-x-y} \\ Cu^{+}(H_2O)_{5-x-z}\,OH^- \end{matrix}\right\} \overset{e^-}{\Leftrightarrow} Cu\,(0) \qquad [5]$$

Such a mechanism involves a chemical reaction (C), in this case the dehydration of the water molecule shell surrounding Cu(II); an electron transfer (E), the reduction of Cu(II) to Cu(I); a second chemical reaction (C), the hydrolysis or dehydration of Cu(I); and a second electron transfer step (E), the reduction of Cu(I) to Cu metal.

Of the two electron transfer steps involved in copper reduction, the first (reaction 3) is reported as rate-limiting.[12,13] Under certain conditions, such as near neutral pH electrolytes, copper electroreduction signals only exhibit one electron transfer event.[14]

Subsequent researchers have built upon this mechanism,[15,16] taking into account the intermediate chemical reaction steps related to dehydration (deaquation of solvation shells, reaction 2 and 4[11,17–18]). Reaction 5 needs particular attention since it is the step leading to actual metal deposition, and has been reported to occur via copper (I) ion adsorption prior to its reduction.[19] Certain aspects of copper reduction kinetics remain highly contested, especially when comparing electrolytes of various pH,[14] partially due to difficulty in discerning the second electron transfer (reaction 5). The ability to make such comparisons is essential in order to identify the role of additives, e.g. Fe(II) ions.

The present study therefore aims at identifying a characteristic electrochemical signal relevant to each of the electron-transfer reactions, in order to better understand how the chemical conditions can ultimately affect the mechanism of copper adatom production (reaction 5).

*Electrochemical Society Active Member.
[z]E-mail: allanore@mit.edu

Table I. Experimental conditions investigated. Redox potentials are calculated using standard redox data available in Ref. 31, assuming unit activity for all species except the metal ions, for which activity is taken to be equal to concentration.

Solution	1a	1b	1c	2a	2b	2c	3	4
H_2SO_4 (M)	1.840	1.080	0.890	1.840	1.080	0.890	1.840	1.840
Cu(II) (M)	0.630	0.630	0.630	0.630	0.630	0.630	0.010	0.010
Fe(II) (M)	-	-	-	0.054	0.054	0.054	-	0.054
Temperature (K)	298	298	298	298	298	298	273	273
Expected E Cu^{2+}/Cu (V/SHE)	0.334	0.334	0.334	0.334	0.334	0.334	0.286	0.286
Expected E Fe^{2+}/Fe (V/SHE)	–	–	–	−0.515	−0.515	−0.515	–	−0.509
AC amplitude (mV)	160	160	160	160	160	160	80	80
AC frequency (Hz)	7.75	7.75	7.75	7.75	7.75	7.75	7.75	7.75

Very few studies report the use of alternating current methods, including alternating current voltammetry (ACV), for copper electrodeposition.[16] The advantages of ACV methods were put forward by Smith,[20] and more recent works by Bond have popularized the technique.[21] In ACV measurements, an AC waveform, such as a sine wave, is superimposed onto a linear DC potential sweep. The current response can then be converted into the frequency domain via a Fast Fourier Transform (Supplementary Figure S1). In a plot of power versus frequency, the DC component of the current response is given by a sharp peak near zero frequency. Additional peaks, occurring at multiples of the AC wave's frequency, called the harmonics, represent the AC components of the current response.[20] These individual peaks can be isolated and converted back into the time domain to separately look at the current contribution of each harmonic.[21] The phenomena involved in copper electrodeposition can be separated into faradaic, e.g., charge transfer, and non-faradaic components, e.g., double layer capacitance. Because faradaic processes respond to voltage in a nonlinear fashion, and non-faradaic processes respond linearly, it is possible to separate the two processes using AC techniques.[1] The linear terms, i.e. the non-faradaic processes caused by double layer capacitance effects, will only be present in the DC current response and the first fundamental harmonic AC response.[21,23] Higher harmonics therefore allow examination of charge transfer kinetics without interference from non-faradaic components. In addition, ACV techniques are useful in examining very fast kinetic reactions.[21] ACV therefore typically allows for electrode phenomena not easily seen in DC voltammetry methods to be investigated.[22–24] ACV seems then appropriate for studying copper deposition because of the subsequent electron transfer reactions involved, as well as a possible adsorption step prior to metal deposition which is presumably very fast.

Few predictions are available as to the expected AC current response when adsorbed species are involved,[25] and the authors were not able to find theoretical or experimental studies on the AC voltammetry current response during copper electrodeposition.

This work aims at identifying and characterizing the multiple steps involved in copper electrodeposition in sulfuric acid electrolyte, with particular attention to the effect of Fe(II) ions on deposition kinetics. Technically, and in order to exhibit evidence of the effects on kinetics, ACV is used to investigate the electrochemical mechanism of copper electrodeposition.

Procedures and Experimental Methods

Experimental setup.— A double-walled glass container was used as the electrochemical cell hosting a three-electrode setup. The working electrode was a 6.58 mm diameter rotating copper disk (surface area 0.34 cm^2), polished to a mirror with 1 micron alumina. The electrode was rotated at 800 revolutions per minute in experiments seeking controlled and forced mass transfer conditions. A coiled platinum wire and a saturated calomel electrode (0.241 V vs. SHE at 298 K) were used as counter and reference electrodes, respectively. All potentials are hereafter reported with respect to the standard hydrogen electrode. Solutions were prepared using reagent-grade sulfuric acid (95-98% purity, Sigma-Aldrich), copper (II) sulfate pentahydrate (99% purity, Alfa Aesar), and iron (II) sulfate pentahydrate (99+% purity, Alfa Aesar), and deionized water (100% purity, RICCA Chemical). Powders were weighed first, to obtain the necessary amount of cupric and ferrous ions, and then dissolved over a twenty-four hour period into a solution with the desired molarity of sulfuric acid.

Experiments were either performed at ambient temperature, 298 ± 5 K, or at water's freezing point, 273 K. For the latter, temperature was controlled by flowing ice water through the cell wall. Nitrogen gas was bubbled through all electrolytes for at least 10 minutes prior to electrochemical measurements. A summary of experimental solutions and conditions is presented in Table I.

Each run first consisted in recording the electrochemical impedance at the open-circuit potential to determine the uncompensated ohmic resistance. This value was obtained as the real component of the impedance measured when the imaginary component crosses the real axis on a Nyquist plot, typically for a frequency of around 100 kHz. The measured resistance was used to obtain the actual working electrode potential in post-experiment analysis, and all potential data are reported with such correction.

Measurements with a rotating working electrode were conducted for no more than 5 potential cycles with each freshly polished electrode. Non-rotating experiments were only run for one cycle. Except where noted, all data presented hereafter are with rotation of the cathode. The investigated potential range and the rotation rate were optimized to limit the hydrogen evolution reaction, to limit anodic dissolution of the copper electrode, and to ensure repeatability between cycles in both the DC component and higher AC harmonics. The scan-rate was limited to a fairly fast value in order to limit copper growth during each cycle. Only the third, fourth, and fifth cycles were analyzed. At the end of the last cycle, the cell was dismantled and the electrode was re-polished before the next run.

Methods of data collection and analysis.— The direct current voltammograms were generated using a potentiostat (Reference 3000: Gamry Instruments, USA). For alternating current measurements, a sine wave created with a waveform generator (MOTU UltraLite-mk3 Hybrid: MOTU, USA) was superimposed onto the direct current ramp. The current response was collected using a data acquisition system (DT9837B: Data Translation, USA) at a 25 kHz acquisition frequency. A custom designed code (ver. 5.5.2; Scilab Enterprises, France) was used to analyze the results post-measurement. The complex current response was analyzed using a Fast-Fourier Transform (FFT), which presented a power spectrum with sharp peaks at multiples of the frequency of the AC sine wave (see Supplementary Figure S1). These peaks represented the transformed DC, fundamental, and higher harmonic components, and were isolated and converted back into the time domain using an inverse FFT. Thus, the DC and harmonic results could be individually plotted versus the DC potential.[21]

In absence of a full ACV model for the electrodeposition mechanism of copper, which presumably involves adsorption, the measured AC components were compared to a model drawn from experimental results for a simpler case: a reversible, single electron transfer system involving the ferri/ferrocyanide redox couple with 10 mM $Fe(CN)_6^{3-}$ and 3 M KCl (see Supplementary Figure S2), with the overall reaction:

$$Fe(CN)_6^{3-} + e^- \rightarrow Fe(CN)_6^{4-} \quad [6]$$

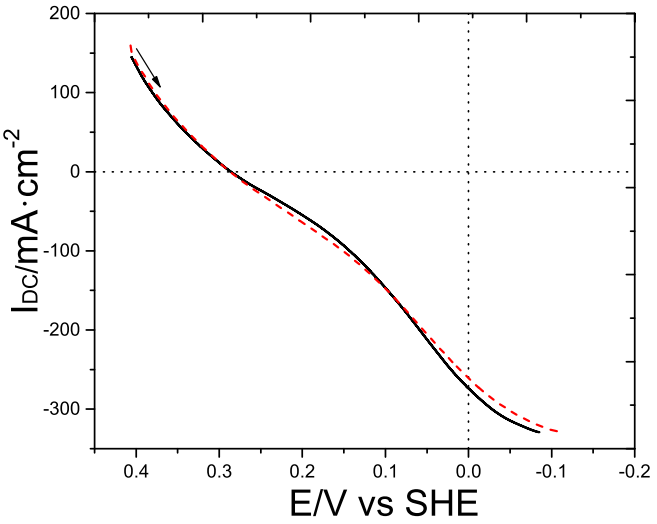

Figure 1. Variation of the direct current during a potential sweep from +0.400 V to −0.100 V in 1.84 M H_2SO_4 and 0.63 M Cu(II) at ambient temperature, without (solution 1a, black, solid) and with 0.054 M Fe(II) (solution 2a, red, dotted). Scan rate is 50 mV.s^{-1}.

This reaction allows investigating a situation where the reaction-rate is quasi-reversible, highly dependent on mass-transfer, and the kinetics are relatively fast, features that are likely to be present in some steps of copper electrodeposition. Under these conditions, the fundamental harmonic presents one sharp, symmetrical peak at the half wave potential, $E_{1/2}$. The second harmonic is represented by the derivative of the fundamental harmonic, with two symmetrical peaks and a trough at $E_{1/2}$. The third harmonic is a derivative of this second harmonic, with three peaks, the middle peak being located at $E_{1/2}$. This pattern repeats for all higher harmonics.[20] In this well-studied system, peak heights scale proportionally with an increase in the electron transfer coefficient, α, and with a faster rate constant k_0. A large α favors more symmetrical peaks, in both height and shape.[22] Four main features are thus of interest in analyzing experimental results: peak heights on both the anodic and cathodic sides of $E_{1/2}$, peak shape symmetry with respect to $E_{1/2}$, overall peak height, and the location of $E_{1/2}$.

Results

Electrodeposition in concentrated solutions at 25°C (fast kinetic conditions).— Figure 1 shows the DC signal measured during copper electrodeposition in a solution with 0.63 M Cu(II) and 1.84 M H_2SO_4, concentrations representative of industrial practices. Multiple analyses of the DC component do not allow for a clear distinction between the current responses for solutions with and without 0.054 M Fe(II).

In ACV signals, as shown in Figure 2, the fundamental and higher harmonic components reveal harmonic peaks characteristic of a faradaic event, for all concentrations of H_2SO_4 (solutions 1a, 1b, 1c, Table I). The peak center for this faradaic event shall henceforth be denoted E_1. E_1^{ω}, as observed for the fundamental harmonic, does not align with $E_1^{2\omega}$, $E_1^{3\omega}$ and $E_1^{4\omega}$ as observed in higher harmonics. The latter are positioned at 0.285 V/SHE across compositions and harmonics, while E_1^{ω} shifts toward a more cathodic potential with an increasing concentration of H^+.

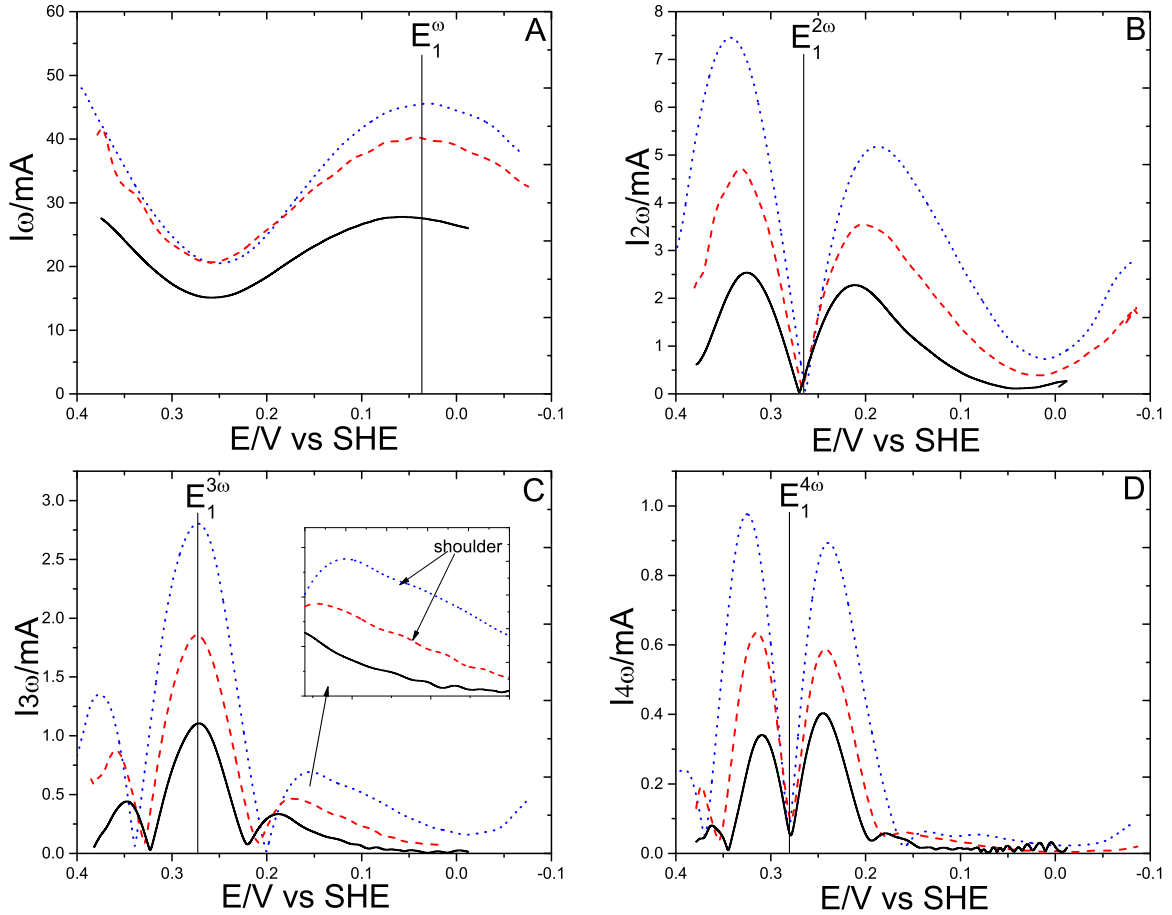

Figure 2. Variation of A) fundamental B) second C) third and D) fourth harmonic current with the DC potential for solutions 1a (blue, dotted, 1.84 M H_2SO_4), 1b (red, dashed, 1.08 M H_2SO_4) and 1c (black, solid, 0.89 M H_2SO_4) at room temperature.

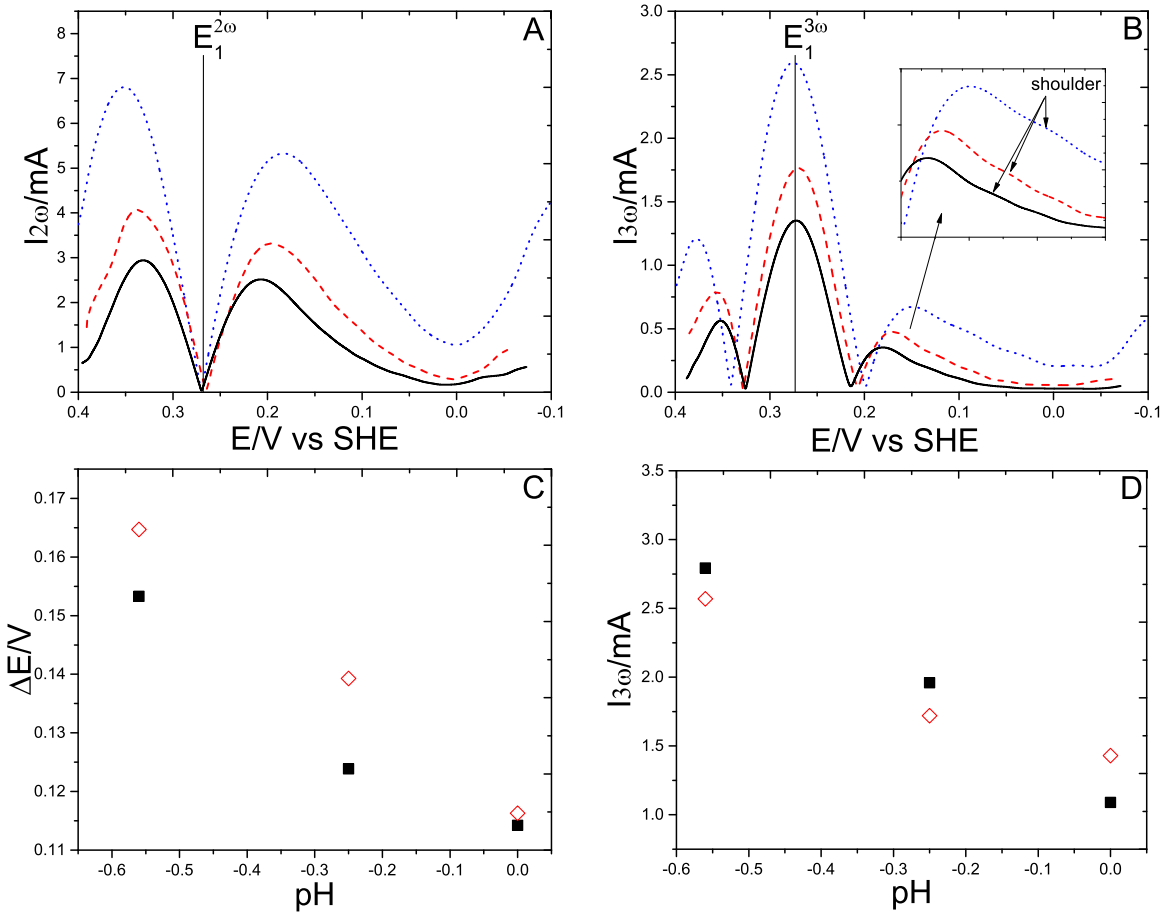

Figure 3. Variation of the A) second and B) third harmonic current with potential for solutions 2a (blue, dotted, 1.84 M H_2SO_4), 2b (red, dashed, 1.08 M H_2SO_4) and 2c (black, solid, 0.89 M H_2SO_4). C) Variation of the difference in the potential for the second harmonic current peaks (see A) and D) Variation of the peak currents at E_1 for the third harmonic current peaks (see B) with pH for solutions without (black, closed) and with 0.054 M Fe(II) (red, open).

In solutions with higher concentrations of H^+, the peak heights become asymmetric with respect to E_1. In 1.84 M H_2SO_4, there is a considerable peak height difference between the two peaks of the second harmonic. In the third and fourth harmonic, the peaks that occur on the anodic side of E_1 are generally higher than their cathodic counterparts, with the exception of the fourth harmonic in the extreme case of 0.84 M H_2SO_4.

The peak shapes are also asymmetrical with respect to E_1. In solutions with higher concentrations of H^+, the peaks at potentials cathodic to E_1 have a prominent shoulder around 0.150 V/SHE (see inset in Figure 2C), which is absent from their anodic counterpart.

Figures 3A and 3B shows the second and third harmonics for solutions that contained Fe(II) ions at 0.054 M (solutions 2a, 2b and 2c, Table I). The measurements of the fundamental harmonic for such solution (not shown) did not exhibit noticeable difference from the one measured for a solution free of iron presented in Figure 2A. In particular, they also exhibit a peak for E_1 at around 0.043 V/SHE. Other key features of the AC harmonics discussed above for solutions without Fe(II) (Figure 2) were more pronounced in solutions containing Fe(II). This is illustrated by the prominence of the shoulder at 0.150 V/SHE in such solutions (see inset Figure 3B). Likewise, the peak heights are more asymmetric than in solutions without Fe(II). Such solutions also show wider harmonics peaks, with the anodic and cathodic sides located further from each other (Figure 3C). In solutions with high concentrations of H^+, peak heights were lower when Fe(II) ions were present (Figure 3D). As with peak distance, this effect is less pronounced at a higher pH.

Electrodeposition in diluted copper solutions at 0°C (slow kinetic conditions).— In order to investigate the possibility that the peak shoulder located at 0.150 V/SHE in Figure 2 was a second faradaic event, efforts were made to slow down electron transfer kinetics. The next set of experiments diverged from previous conditions in favor of a colder temperature (273 K) and a lower concentration of Cu(II). These solutions (solutions 3 and 4, Table I) were prepared with 0.01 M Cu(II) and 1.84 M H_2SO_4, both with and without 0.054 M Fe(II). Cyclic voltammetry experiments under these conditions (Figure 4) still do not show a significant difference between solutions with and without Fe(II).

Figure 5 is an overlay of the fundamental and second harmonic from a solution at 273 K containing 0.01 M Cu(II), 1.84 M H_2SO_4 and 0.054 M Fe(II). As anticipated for such conditions, lower AC currents are measured, indicative that reaction rates were slower. Two separate faradaic events can be observed, at 0.33 V/SHE and 0.04 V/SHE, termed E_1 and E_2, respectively. These two distinct fundamental harmonic peaks line up with two distinct second harmonic troughs. The location of E_1^{ω} at low temperature (Figure 5) is shifted anodically compared to the room temperature data such that it is now aligned with E_1 observed for the higher harmonics.

Figure 6 shows the harmonics for the isolated first and second faradaic events. With the exception of the E_1 offset by around 25 mV, no significant difference in peak height or shape are observed for this event in solutions with or without Fe(II). In presence of Fe (II), E_2 (Figure 6, insets) is more cathodic and separated from E1, with consistently lower harmonic peaks and more distinctive features than in absence of Fe(II). Compared to the harmonics at E_1, and the results of the ACV model (see Appendix 2), the E_2 peaks are atypical. $E_2^{3\omega}$ and $E_2^{4\omega}$ are located at a more cathodic potential than E_2^{ω} or $E_2^{2\omega}$. This shift is similar to the one observed in Figure 2A, where the location of E_1 shifts between the fundamentals and the higher

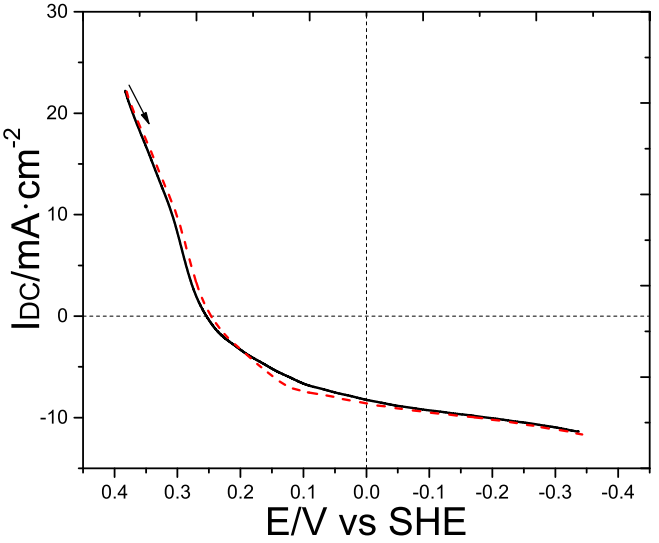

Figure 4. Variation of the direct current during a potential sweep from +0.400 V to −0.350 V in 1.84 M H_2SO_4 and 0.01 M Cu(II) at 273 K, without (solution 3, black, solid) and with 0.054 M Fe(II) (solution 4, red, dotted). Scan rate is 50 mV.s^{-1}.

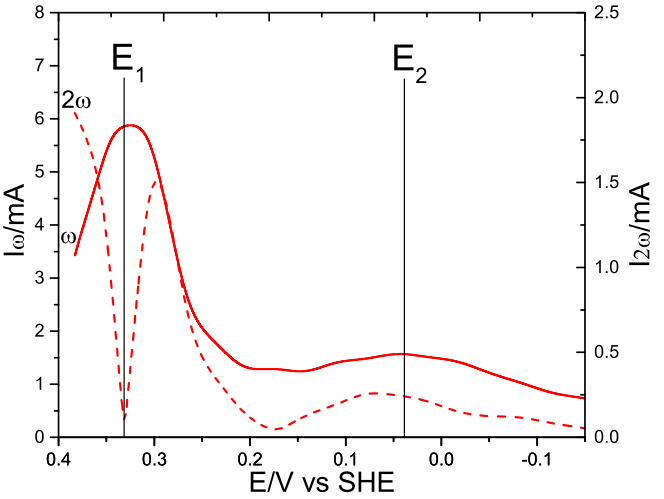

Figure 5. Overlaid fundamental (red, solid) and second (red, dashed) harmonic current response for solution 4 (0.01 M Cu(II), 0.054 M Fe(II), and 1.84 M H_2SO_4) at 273 K.

harmonics. The observed faradaic event at E_2 is distorted towards more anodic potentials due to overlap with the faradaic event at E_1, with the strongest effect on the fundamental harmonic. Higher harmonics appear less susceptible to such overlap, pertaining more strictly to the charge transfer of interest, with peak positions stabilizing in the third and fourth harmonic.

Although the peaks at E2 (Figures 6c and 6d) are strongly asymmetrical, they split at a consistent potential with alternating peaks (for odd harmonics) and troughs (for even harmonics). This is a definitive characteristic of a faradaic event in AC voltammetry, with the observed asymmetry being typical of an irreversible reaction.[20,25] Such a

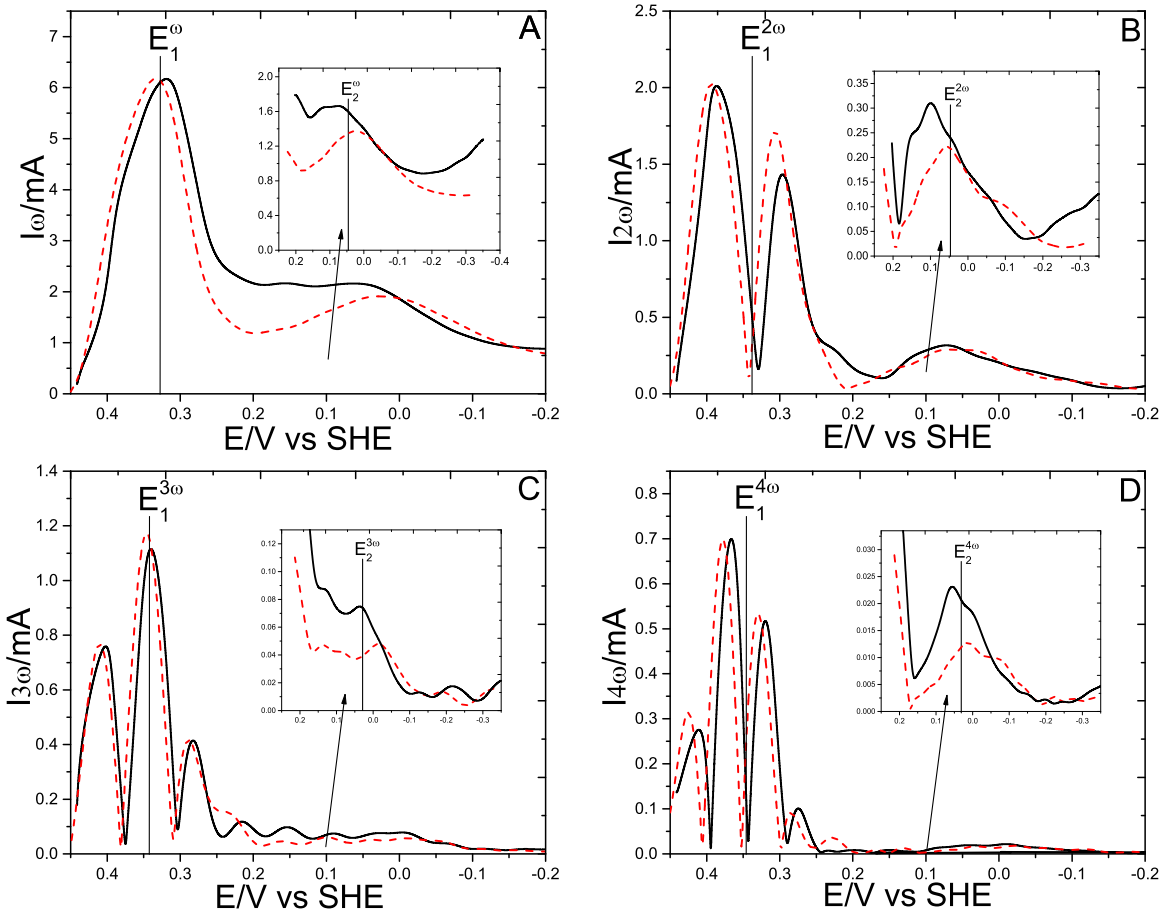

Figure 6. Variation of A) fundamental B) second C) third and D) fourth harmonic current with the DC potential for experiments in 1.84 M H_2SO_4 and 0.01 M Cu(II) at 273 K, without (solution 3, black, solid) and with 0.054 M Fe(II) (solution 4, red, dotted).

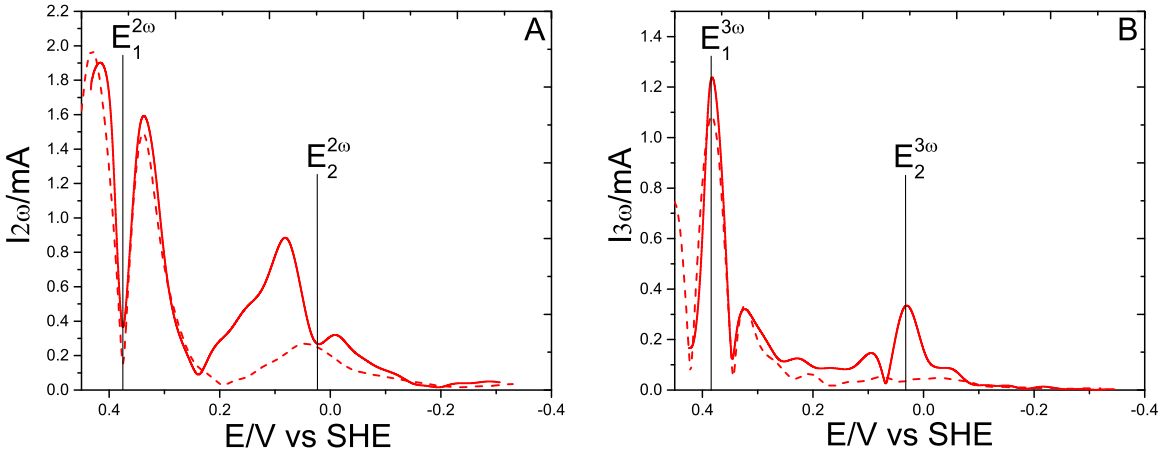

Figure 7. Variation of A) second and B) third harmonic current with the DC potential for experiments in solution 4 (0.01 M Cu(II), and 0.054 M Fe(II), and 1.84 M H_2SO_4) at 273 K, without (red, solid) and with rotation at 800 rpm (red, dotted).

current response shape has also been predicted for reactions involving an adsorption step.[25]

In order to further investigate the electron transfers occurring at E_1 and E_2, measurements conducted in absence of rotation of the working electrode are reported (Figure 7). The absence of rotation did not affect the E_1 signals, while peak currents at E_2 increased and the peak split in higher harmonics is more pronounced. Furthermore, the harmonics at E_2 in absence of rotation exhibit a similar shape to E_1, and are in more qualitative agreement with the ACV model.

Discussion

Copper electroreduction mechanism.— Depending on the experimental conditions highlighted earlier, one or two faradaic events may be distinguished during copper electrodeposition. In industry-level concentrations and at room temperature, DC measurements indicate an inflection point at 0.25 V/SHE (Figure 1), a distinct event E_1 also observed in AC measurements in second and higher harmonics. At lower temperatures and lower copper concentration, the location of E_1 shifts anodically, as would be expected from a system with Nernstian behavior. The location of E_1 at a potential close to the standard electrode potential for Cu(II) reduction to Cu metal (Table I), and the lack of any other thermodynamically possible faradaic reactions occurring at that potential lead us to assign E_1 to the following reaction:

$$Cu^{2+} \overset{e^-}{\Leftrightarrow} Cu^{+} \qquad [3]$$

This first step, according to the previous literature, is the slowest faradaic step in the overall copper electrodeposition reaction. DC measurements in industrial concentrations also indicate a second inflection point at 0.05 V/SHE, E_2 (Figure 1), an event not noticed as clearly as E_1 in AC measurements under the same conditions. Instead, the second and third harmonic currents from E_1 exhibit shoulders overlapping with the current response at E_2. The shoulders are most prominent in low pH solutions, which have been shown to be associated with a smaller α.[11,26] The loss of peak symmetry could be attributed to a decrease in α, or to the increasing prominence of the event at E_2. Slowing overall reaction kinetics, either through decreasing pH, decreasing Cu(II) concentration, or decreasing temperature, point to slower events at E_1 and E_2, increasing the prominence of the shoulder. Furthermore, at low pH, the harmonics for E_1 are more asymmetrical, again indicating overlap with the currents from E_2. This overlap is consistent with ACV models for multiple electron transfer steps.[20]

In the extreme case shown in Figures 5 and 6, the two reduction steps at E_1 and E_2 are completely separated. In these cold solutions with low concentrations of Cu(II), no shoulders on the cathodic side of the reaction are observed. This confirms that the second event corresponds to a distinct electron transfer reaction, and that the shoulders observed under industrial conditions are due to the overlap of E_1 and E_2 currents. It is likely, therefore, that the event E_2 is very fast compared to E_1, such that it is often masked by E_1 current responses. The event E_2 exhibits atypical second and higher harmonic currents exhibiting strongly asymmetrical shapes, pointing to an irreversible reaction or a reaction involving an adsorbed species.[20,25]

It is possible that the hydrogen evolution reaction (HER) occurs in parallel with the reaction at E_2, although studies of hydrogen evolution on copper electrodes report large overpotentials for HER.[4,5,27] Furthermore, Fe(II) ions have been shown to be a catalyst for HER,[27] which contradicts the decrease in currents observed for E_2 in systems in the presence of Fe(II) (Figure 6).

Results with a stationary working electrode show that the ACV signal at E_2 has a stronger dependence on rotation than at E_1, with the event E_2 appearing more distinct and better defined in absence of rotation (Figure 7). For a mass-transfer controlled quasi-reversible reaction, ACV signals have been shown to be insensitive to the mass-transfer conditions for low-enough frequencies of excitation.[28] This result applies to our AC measurements for reaction 3 at E_1, which involves soluble species and did not exhibit variation with or without rotation. Nevertheless, it can be postulated that in absence of rotation, the soluble product (Cu(I)) for reaction 3 stays in the vicinity of the electrode and is less dispersed toward the bulk of the electrolyte. Such Cu(I), confined to the electrode surface is then more available for further reaction, explaining the enhanced AC signal at E_2.

The faradaic event E_2 therefore appears as a second electron transfer step involving surface confined species, most likely following reaction 5:

$$Cu^{+} \overset{e^-}{\Leftrightarrow} Cu \qquad [5]$$

Previous authors have reported such a reaction occurring at similar potentials, suggesting that the reaction involves Cu(I) as an adsorbed species and is a very fast electron transfer reaction.[18] Such a scheme is in agreement with the mechanism presented in introduction, with reaction 5 involving surface species, e.g. adsorbed species. That reaction 5 can be affected by the amount of Cu(I) supplied from reaction 3 and possibly the mass-transfer conditions is a feature that can be evidenced thanks to the combination of ACV and RDE techniques.

The features of the fundamental harmonics for copper electrodeposition recorded in proton concentrated solutions remain anomalous, in particular with regards to the shift of $E_1{}^{\omega}$ from the Nernst reduction potential for reaction 1. Such a shift is not observed in conditions where reaction 5 can be isolated (see Figure 2 vs Figure 5 for example), suggesting that the measured reduction potential for reaction 1 in industrial-simulating concentrations represents a value between the Nernst potentials for reactions 1 and 2. This is also consistent

with ACV models for a mechanism involving two successive electron transfer steps.[20]

Influence of Ferrous Ions.— In very acidic solutions, the influence of Fe(II) on the electron transfer kinetics is more predominant at low pH. With Fe(II) present in the electrolyte, the harmonic peaks for reaction 3 remain strongly asymmetrical, even at a higher pH, as opposed to measurements without Fe(II). This suggests that reaction 5, which has harmonics better resolved in solutions with high concentration of proton, is influenced by Fe(II), the presence of which enhances the separation between reaction 3 and 5 (see Figures 3A and 3B).

Under conditions where the two reduction steps are distinguishable, no difference in harmonic shape for reaction 3 in solutions with and without iron can be observed (Figure 6). Conversely, reaction 5 is highly influenced by the presence of Fe(II) (Figure 6, insets). Measurements in solutions containing Fe(II) reveal consistently decreased current values; and peak shapes that more qualitatively fit the ACV model than measurements without Fe(II).

When Fe(II) is present in the system, reaction 3 appears at more anodic potentials, while reaction 5 occurs at more cathodic potentials. Fe(II) ions therefore appear to be hindering reaction 5, thus enhancing separation between the two electron transfers, while not influencing reaction 3. Those results are a key step in isolating and studying the two reactions independently, and in ultimately extracting kinetic parameters for Cu(II) reduction.

Our results allow us to support the hypothesis that the electron transfers in copper reduction obey the following mechanism:

$$step\ 1 \qquad Cu^{2+} \overset{e^-}{\Leftrightarrow} Cu^{+}$$

$$step\ 2 \qquad Cu^{+} \Leftrightarrow Cu^{+}_{ads}$$

$$step\ 3 \qquad Cu^{+}_{ads} \overset{e^-}{\Leftrightarrow} Cu^{0}_{ads}$$

The inconsistent trends with pH for step 3 (reaction 5), however, may also indicate that Fe(II) affects the intermediate chemical reaction 4:

$$Cu^{+}(H_2O)_{6-x} \overset{-yH_2O}{\Longleftrightarrow} Cu^{+}(H_2O)_{6-x-y}$$

in which case water solvation shell interactions between Fe(II) and Cu(I) would have to be studied.

Lack of a fully developed model for ACV experiments on such mechanism involving adsorption limits the extent to which kinetics for Cu(I) reduction and the influence of Fe(II) on this reduction can be quantitatively characterized. It is suggested that future work be focused on developing such a model.

Conclusions

The overall currents measured in DC and AC voltammetry in industry-emulating concentrations are the combination of currents from Cu(II) reduction to Cu(I), and Cu(I) reduction to Cu metal. In conditions designed to slow charge transfer kinetics, these two reduction steps can be separately observed by ACV. The shapes of the harmonic current peaks for Cu(I) reduction support previous reports that Cu(I) reduction occurs as an adsorbed species. In strongly acidic conditions, Fe(II) lowers the overall reaction kinetics measured in DC and AC voltammetry. ACV results show that Fe(II) has a stronger effect on Cu(I) reduction, producing lower peak currents at larger overpotentials. According to electrocrystallization theory, such limitation of the deposition rate for Cu in presence of Fe (II) may be responsible for the morphological features of the deposit growth reported in the past.

Acknowledgments

The author acknowledge the MISTI-Chile program for its financial support throughout this project.

References

1. T. C. Liu, C. M. Liu, Y. S. Huang, C. Chen, and K. N. Tu, *Scr. Mater*, **68**, 241 (2013).
2. Y. Liu et al., *IEEE Trans. Components Packag. Technol.*, **33**, 127 (2010).
3. F. Qiao, B. B. O'Brien, K. A. Dunn, and A. C. West, *J. Electrochem. Soc.*, **160**, D271 (2013).
4. N. D. Nikolić, G. Branković, M. G. Pavlović, and K. I. Popov, *J. Electroanal. Chem.*, **621**, 13 (2008).
5. N. D. Nikolic, *ZAŠTITA Mater*. **51** (2010).
6. T. Vargas and P. Parra, *International Copper Conference*, Volume 5, Book 1, Editors R. Abel and C. Delgado, p. 51 (2014).
7. Z. D. Stanković, V. Cvetkovski, and M. Vuković, *J. Min. Metall. Sect. B Metall.*, **44**, 107 (2008) http://www.doiserbia.nb.rs/Article.aspx?ID=1450-53390801107S#.VTpWua3BzGd.
8. M. A. Pasquale, L. M. Gassa, and A. J. Arvia, *Electrochim. Acta*, **53**, 5891 (2008) http://www.sciencedirect.com/science/article/pii/S0013468608004799.
9. Z. D. Stanković, *J. Electrochem. Soc.*, **128**, 1862 (1981).
10. Z. D. Stanković, *Electrochim. Acta*, **29**, 407 (1984) http://www.sciencedirect.com/science/article/pii/0013468684870838.
11. J. L. Anderson and I. Shain, *Anal. Chem.*, **48**, 1274 (1976).
12. J. O. Bockris and M. Enyo, *Trans. Faraday Soc.*, **58**, 1187 (1962) http://pubs.rsc.org/en/content/articlehtml/1962/tf/tf9625801187.
13. E. Mattsson and J. O. Bockris, *Trans. Faraday Soc.*, **55**, 1586 (1959).
14. A. A. Shaikh, J. Firdaws, J. Badrunnessa, S. Serajee, M. S. Rahman, and P. K. Bakshi, *Int. J. Electrochem. Sci.*, **6**, 2333 (2011) http://www.electrochemsci.org/papers/vol6/6072333.pdf.
15. T. Hurlen, G. Ottesen, and A. Staurset, *Electrochim. Acta*, **23**, 39 (1978) http://www.sciencedirect.com/science/article/pii/0013468678870315.
16. S. Venkatesh, *J. Electrochem. Soc.*, **128**, 2588 (1981).
17. J. L. Anderson and I. Shain, *Anal. Chem.*, **50**, 163 (1978).
18. L. M. C. Pinto, P. Quaino, E. Santos, and W. Schmickler, *ChemPhysChem*, **15**, 132 (2014) http://www.ncbi.nlm.nih.gov/pubmed/24376128.
19. J. Vazquez-Arenas, *Electrochim. Acta*, **55**, 3550 (2010).
20. D. E. Smith, in *Electroanalytical Chemistry: A Series of Advances (I)*, A. J. Bard, Editor, p. 1, Marcel Dekker, Inc., New York (1966).
21. A. M. Bond, N. W. Duffy, S.-X. Guo, J. Zhang, and D. Elton, *Anal. Chem.*, **77**, 186A (2005).
22. A. A. Sher, A. M. Bond, D. J. Gavaghan, K. Harriman, Stephen W. Feldberg, N. W. Duffy, S. X. Guo, and J. Zhang, *Anal. Chem.*, **76**, 6214 (2004) http://www.ncbi.nlm.nih.gov/pubmed/15516112.
23. E. Mashkina, T Peachey, C. Lee, A.M. Bond, G. F. Kennedy, C. Enticott, D. Abramson, and D. Elton, *J. Electroanal. Chem.*, **690**, 104 (2013).
24. M. J. A. Shiddiky, A. P. O'Mullane, J. Zhang, L. D. Burke, and A. M. Bond, *Langmuir*, **27**, 10302 (2011).
25. W. H. Reinmuth, *Anal. Chem.*, **40**, 185 (1968).
26. L. W. Yip, thesis, University of Hong Kong (1983).
27. J. Fuentes-Aceituno and G. Lapidus, in *XI International Hydrogen Congress*, p. 1 (2011).
28. K. Tokuda and H. Matsuda, *J. of Electroanal. Chem.*, **90**, 149 (1978).
29. J. W. Dini, *Electrodeposition - The Materials Science of Coatings and Substrates*, Noyes Publications, Westwood, (1993).
30. M. Paunovic and M. Schlesinger, in *Fundamentals of Electrochemical Deposition*, p. 77, John Wiley & Sons, Inc. (2006).
31. A. J. Bard and L. R. Faulkner, *Electrochemical Methods- Fundamentals and Applications*, Second., J. Wiley, New York, (2001).